Journal of Colloid and Interface Science **241,** 317–326 (2001)
doi:10.1006/jcis.2001.7773, available online at http://www.idealibrary.com on IDEAL®

ATR–FTIR Spectroscopic Investigation on Phosphate Adsorption Mechanisms at the Ferrihydrite–Water Interface

Yuji Arai[1] and D. L. Sparks

Department of Plant and Soil Sciences, University of Delaware, Newark, Delaware 19717-1303

Received April 3, 2001; accepted June 8, 2001; published online August 8, 2001

We investigated the phosphate(P) adsorption mechanisms at the ferrihydrite–water interface as a function of pH, ionic strength (I), and loading level, using a combination of adsorption envelopes, electrophoretic mobility (EM) measurements, and attenuated total reflectance Fourier transform infrared (ATR–FTIR) spectroscopy. The P adsorption envelopes show that: (1) adsorption decreases with increasing pH 3.5–9.5 and (2) adsorption is insensitive to changes in I at pH 4–7.5, but it slightly increases with increasing I from 0.01 to 0.8 at pH $>$ 7.5. The EM in 0.1 M NaCl decreases with increasing P concentration from 0 to 50 μmol L^{-1} at pH 3–9. The results of these macroscopic studies suggest the formation of inner-sphere complexes. The ATR–FTIR investigation shows that inner-sphere surface complexes are nonprotonated, bidentate binuclear species ($\equiv Fe_2PO_4$) at pH $\geq$ 7.5 and could be associated with Na^+ ions at P loading levels of 0.38 μmol m^{-2}. At pH 4–6, protonated inner-sphere complexes are proposed at the loading levels between 0.38 and 2.69 μmol m^{-2}.

Key Words: **phosphate; adsorption; ionic strength; ferrihydrite; surface complexation; electrophoretic mobility; ATR–FTIR.**

INTRODUCTION

In the past few decades, excess P has been recognized as a nonpoint-source agricultural pollutant throughout the world due to the overapplication of both synthetic and animal based fertilizers (1, 2). In 1996 the USEPA reported that more than 50% of freshwater eutrophication is attributed to agricultural nutrients such as P. Eutrophication as well as the overgrowth of cyanobacteria due to the excess P in recreational, industrial, and drinking water could greatly threaten human and ecological health. Therefore, the fate and transport of P in soil/water environments must be well understood to design effective remediation strategies for reducing negative impacts on aquatic/terrestrial environments. Various abiotic and biotic factors (pH, redox, ionic strength, adsorbent type, percentage organic matter content, temperature, concentration, competitive adsorbates, solubility product effects, and nonreductive/reductive dissolution of adsorbate) greatly affect the reactivity, speciation, mobility, and bioavailability of P. Because adsorption to mineral surfaces is one of the most important rate-limiting factors controlling P release in subsurface environments, it is vital to study the mechanisms of P adsorption on naturally occurring soil minerals.

Many researchers have investigated P adsorption mechanisms on major soil minerals (e.g., iron oxides) using in situ/ex situ Fourier transform infrared (FTIR) spectroscopy. While the predominant formation of inner-sphere bidentate binuclear complexes on ferrihydrite, goethite, lepidocrocite, and hematite was suggested by several researchers (3–8), the inner-sphere monodentate mononuclear complexes at the goethite surface were later proposed (9).

An important factor accounting for the differences in the proposed P surface complexes on iron oxides between the previous studies may lie in the use of (i) different FTIR techniques (e.g., in situ versus ex situ FTIR spectroscopy) and (ii) different data interpretation processes (e.g., molecular symmetry assignment of adsorption complexes based on asymmetric v^3 vibration or peak position comparison with iron phosphate model complexes). Evidence of inner-sphere complexation in the ex situ (dry and severely evacuated sample conditions) studies has been questioned by many researchers due to the possible creation of artifacts (i.e., a structural alteration by drying the residual adsorbate and removal of entrained water). In situ spectroscopic investigations are preferred, because the colloidal interfaces in natural settings contain water and are at atmospheric pressure (10). Comparing the peak position between adsorption complexes and model complexes to assign the type of surface complexes can be problematic because the peak position could often shift due to different reaction conditions (e.g., loading level, pH, and moisture content) (3, 6, 8, 12). The molecular symmetry assignment of adsorption complexes based on the asymmetric vibration has been preferably used in recent vibrational spectroscopic studies to investigate oxyanion (arsenate, carbonate, phosphate, selenate, and sulfate) adsorption mechanisms at the mineral–water interface (9, 11–15).

The two-line ferrihydrite (FH) (an amorphous hydrous ferric oxide) was chosen in this study because (i) it commonly forms in soils and sediments (16–19) and (ii) its strong adsorption capacity for P (20, 21) has implications in P agrogeochemical

[1] To whom correspondence should be addressed. E-mail: ugarai@udel.edu. Fax: 302(831)0605.

0021-9797/01 $35.00

cycles in the environment. The presence of P ligands at the FH surfaces are known to retard the transformation of FH into crystalline phases like goethite (22, 23) and might also inhibit reductive/nonreductive dissolution reactions of the FH. The reductive or nonreductive dissolution inhibitory reactions have been documented for P adsorbed on lepidocrocite and goethite surfaces (24, 25). Since the P surface speciation on FH surfaces has been only investigated via ex situ FTIR spectroscopic analysis (7, 26), the reaction dynamics of P ligands at the FH–water interfacial environments are not clearly understood. Therefore the objective of our study was to investigate P surface speciation (i.e., P surface complexation and the protonation environment) at the FH–water interface using in situ, attentuated total reflectance (ATR)–FTIR spectroscopy. Phosphate surface complexes are proposed based on the molecular symmetry assignment via Gaussian profile fit analysis of phosphate υ_3 vibrations. Additionally, the in situ spectroscopic analyses were complimented with macroscopic investigations such as adsorption envelopes as a function of ionic strength (I) and electrophoretic mobility (EM) measurements.

MATERIALS

The two-line ferrihydrite was synthesized according to Schwertmann and Cornell (27). Forty grams of ferric nitrate were dissolved in 500 ml deionized water. The pH of the solution was titrated to pH 7.5 and maintained at this pH value for 45 min by addition of 1 M NaOH. The FH precipitate was washed with deionized water and the supernatant was decanted after centrifugation. This was repeated until the nitrate concentration was reduced to below 0.003 mmol. The FH paste was then freeze dried prior to the adsorption experiments. The five-point, Brunauer–Emmett–Teller (BET) surface area was 260 $m^2\ g^{-1}$. The point of zero salt effect (PZSE), as determined by the potentiometric titration method (28), was 8. Powder X-ray diffraction (XRD) analysis revealed the diagnostic, two peaks for two-line ferrihydrite (0.24 and 0.15 nm).

METHODS

Ionic Strength (I) Effects on P Adsorption Envelopes

Phosphate adsorption envelopes were investigated at different solution ionic strengths (0.8, 0.1, and 0.01 M NaCl). A N_2 filled glove box was used to minimize the pH shifts in the atmospheric CO_2 partitioning. Twenty milliliters of FH suspensions ($\rho = 2\ g\ L^{-1}$) were transferred to 50 ml Nalgene high speed centrifuge tubes. A total of 10 samples were prepared for each value of I. After 2 min of ultrasonification at 60 W, pH values were adjusted to provide a range of 3–10 with addition of 0.1 M HCl or NaOH. The samples were shaken at 150 rpm at 25(±1)°C for 24 h. Next, the samples were spiked with 20 ml of 1.4 mmol P stock solution over the same pH range and I to provide an initial P concentration of 0.7 mmol. The samples were shaken on an orbital shaker at 150 rpm for 24 h. The pH was periodically adjusted with 0.1 M HCl or NaOH. After equilibration, the tubes were centrifuged at 3000 rpm for 10 min. The pH of the supernatant was measured. The filtered supernatants were passed through a 0.2 μm Supor 200 filter and analyzed for dissolved P using the modified molybdenum blue method (29, 30).

Electrophoretic Mobility Measurements

To assure accuracy of the EM measurements, a Zeta-Meter 3.0 system (Zeta Meter, Inc., New York) was calibrated by measuring a constant zeta potential (-29 ± 1 mV) of Min-U-Sil (i.e., standard colloidal silica) in distilled water. Freeze dried FH (suspension density (ρ) = 0.4 g L^{-1}) was hydrated in 30 ml of 0.01 M NaCl solution, and ultrasonified for 2 min at 60 W. The pH was adjusted to the desired pH values (4, 4.75, 5.5, 6.25, 7, 7.5, 8.5, and 9.25) by adding 0.1 M HCl and 0.1 M NaOH. After 24 h of equilibration, the mineral suspensions were reacted with 20 ml of sodium phosphate solutions (62.5 or 125 μmol L^{-1}) over the same pH and I to provide initial P concentrations of 25 and 50 μmol L^{-1}. After 48 h of equilibration, approximately 10 ml of well-mixed suspensions were inserted into the electrophoretic cell. Tracking time measurements of particle movement were repeated for 10 particles. The average value was used to estimate the EM values using the Helmholtz–Smoluchowski equation (31).

Sample Preparation for the ATR–FTIR Analysis

Infrared spectra of adsorbed phosphate on the FH surface were studied as a function of (i) pH (4–9) at constant loading level (i.e., $\Gamma = 0.38\ \mu mol\ m^{-2}$) and (ii) P loading level (0.38–2.69 $\mu mol\ m^{-2}$) at constant pH 4 and 7.5. Hydration and pH adjustments of the FH suspensions were accomplished using the method described in the adsorption envelope section. The final suspension density of 1 g L^{-1} and I = 0.1 M NaCl were used in all experiments. A monodentate mononuclear iron phosphate (aq) reference complex (1.5 M $FeCl_3 \cdot 6H_2O$, 0.75 M Na_2HPO_4 and [OH]/[Fe] = 1) was prepared based on the study by Rose *et al*. (32) to aid in IR spectra data interpretation. The sodium P solution complexes (0.1 M Na_2HPO_4 in 1 M NaCl) at different pH values (1.3, 4.8, 8, and 12.8) were also prepared following the method described in the study by Tejedor-Tejedor and Anderson (8).

Adsorption samples for pH 4 and 7.5 under the 0.38 and/or 2.69 $\mu mol\ m^{-2}$ loading level were also prepared in D_2O under the same reaction conditions above. The preparation of the reagents (0.1 M NaCl and 2 mmol Na_2HPO_4) and the P adsorption experiments in D_2O were performed in the N_2 filled glove box. The FH was hydrated in the 20 ml 0.1 M NaCl in D_2O for 3d. After the hydration, the pH of the suspension was adjusted to 4 or 7.5 for 24 h with 0.1 M DCl and NaOD. The P stock solution (pH 4 or 7.5 and I = 0.1 M NaCl) was added to the mineral suspensions, and then the pD was periodically adjusted for 48 h. The samples were recovered by the centrifugation method described above, and the paste was recovered in the N_2 glove box. To minimize the partitioning of the atmospheric

hydrogen, the paste was quickly loaded on the ATR–FTIR trough and it was continuously purged with N_2 during the FTIR analysis.

ATR–FTIR Analysis

ATR–FTIR data collection was conducted on a Perkin-Elmer 1720x spectrometer equipped with a N_2 purge gas generator and a MCT detector. ZnSe and Ge horizontal crystals (45° angle of incidence) were used for the adsorption samples and the P solution samples (sodium phosphate and iron phosphate solutions), respectively. A total of 500 coadded spectra were collected for the adsorption samples at a resolution of 2 cm^{-1}, and a total of 150 coadded spectra were taken.

All spectra were ratioed against the spectra of an empty cell. Subtraction of the spectra was performed to obtain all final spectra. For example, the final spectra were obtained by subtracting the spectra of the entrained solution and the FH paste or the background solution from the spectra of reacted samples (i.e., P adsorbed iron oxides or P solution, respectively). All spectra were normalized with respect to the highest absorbance (at $\cong$1020 cm^{-1}) of each sample. Since ATR–FTIR spectra subtraction was done at the slope of the absorption band of the ferrihydrite (<1100 cm^{-1}), it is difficult to preserve the P υ_1 vibration at <800 cm^{-1} if present. Therefore the changes in the P υ_3 vibrations are mainly discussed in Results and Discussion.

RESULTS AND DISCUSSION

Ionic Strength Effects on Adsorption Envelopes

Figure 1 shows the effects of ionic strength on P adsorption envelopes. Approximately 70% ($\cong$1.85 μmol m^{-2}) of P was removed at pH $\cong$ 4 at all I, and the net adsorption decreased to 30% ($\cong$0.8 μmol m^{-2}) with pH increasing up to 9.5 (Fig. 1). The P adsorption appears to be insensitive to changes in I between pH 3.5 and 7.5, whereas the adsorption increases with increasing I at pH > 7.5. Ionic strength independent P adsorption behavior on soils (New Zealand loamy soils) and soil components (kaolinite, montmorillonite, illite, and goethite) have been reported by several researchers (33–39).

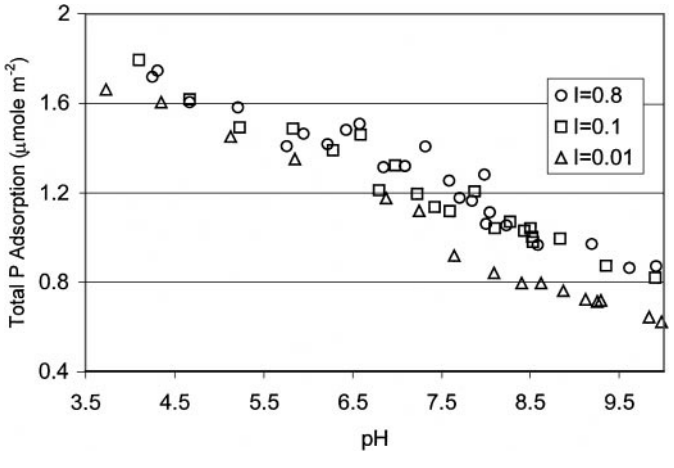

FIG. 1. Ionic strength effects on P adsorption envelopes at the FH–water interface.

Oxyanion adsorption onto variable charge mineral surfaces may form inner-sphere complexes (via ligand exchange) and/or outer-sphere complexes (via electrostatic interaction). These surface complexes can be indirectly distinguished by the I effects on the adsorption envelopes (40). Inner-sphere complexes (i.e., selenite) are insensitive to changes in I, while outer-sphere complexes (i.e., selenate) are sensitive to the changes in I because of competition with counter anions in the background electrolytes. Based on this argument, we can suggest the formation of P inner-sphere complexes at pH 3–7.5. We, however, do not have a straightforward explanation for the increase in the P adsorption with increasing I observed at pH > 7.5. Barrow *et al.* (33) also observed these unique P adsorption phenomena at the goethite–water interface at pH > 4.3. The data were later explained using the quadruple-layer adsorption model (41), but McBride (42) pointed out that the model is not suited to explain the anion adsorption behavior due to the use of the hypothetical fitting parameters. The diffuse double layer theory can also be considered. Decreased double layer thickness due to increased I allows the P ions to approach closer to the negatively charged surfaces, where they form inner-sphere complexes via ligand exchange mechanisms. Inner-sphere adsorption, however, should not be influenced by either the thickness of the diffuse double layer or the repulsion force because the specific adsorption involves direct coordination to discrete surface metal cations (42). Instead, McBride suggested the simple mass action principle to explain the unique P adsorption phenomena. The principle is similar to the constant capacitance model described by Goldberg and Sposito (43). The surface electrical potential correction term is ignored by assuming that any inner-sphere and outer-sphere counter ions are adsorbed to balance the surface charge created in the process. In the case of high I, the negatively charged surfaces created by the inner-sphere P adsorption are likely to be neutralized by co-adsorption of cations (i.e., Na^+) from indifferent electrolytes. Therefore, higher electrolyte concentrations may facilitate the P adsorption via the following reaction:

$$\equiv Fe\text{–}OH + Na^+ + HPO_4^{2-} \rightarrow \equiv Fe\text{–}O\text{–}PO_3H \cdots\cdots Na^+ + H_2O.$$

In fact, there is macroscopic evidence to support this theory. Nanzyo (26) reported that sodium adsorption was significantly enhanced from 0.76 to 1.84 μmol m^{-2} with increasing P adsorption from 0 to 0.8 μmol m^{-2} on iron hydroxide gel at pH $\cong$ 10.

Accordingly, our P adsorption envelope data suggest that P predominantly forms inner-sphere complexes at the FH–water interface at pH 4–9.5. No conclusive statements can be made based on the macroscopic data. We therefore performed the EM measurements and ATR–FTIR analysis of P adsorption at the FH–water interface.

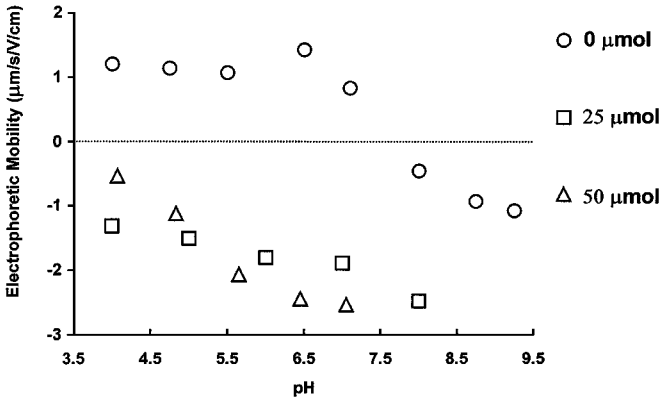

FIG. 2. Electrophoretic mobility measurements on the FH with/without 25 and 50 μmol sodium P solution.

EM Measurements

The EM measurements showed that the presence of 25 and 50 μmol P in 0.1 M NaCl solution lowered the EM between pH 4 and 10 and shifted the isoelectric point (IEP) of the solid from $\cong$8 to $<$4.0 (Fig. 2). Charge reversals in EM and shifts in IEP due to P adsorption to hematite and goethite have been previously reported (8, 44).

According to Hunter (45), the EM measurements are useful not only in obtaining isoelectric points for colloidal materials, but also in indirectly distinguishing inner-sphere complexes from outer-sphere complexes. Nonspecific ion adsorption of indifferent electrolytes outside of the shear plane (i.e., formation of outer-sphere complexes via van der Waals forces) generally does not affect the IEP, but it could cause shifts in the value of EM if the concentrations of indifferent electrolyte are high (45). The shear plane is at the outer edge of the inner part of the double layer and near the outer Helmholtz plane or the Stern layer, depending on the models used to describe the interface (45). Inner-sphere complexes generally cause shifts in both IEP and EM due to specific ion adsorption inside the shear plane (45). In some cases, however, inner-sphere adsorption does not significantly affect the EM and IEP of the pure solid suspension (45, 46).

Based on the information above, our EM measurements suggest the formation of inner-sphere complexes for P at pH 4–9. As mentioned above, EM can be shifted by physically adsorbed anions such as chloride. Moreover the chloride concentration was the same in all EM measurements, so if physical adsorption of chloride is outcompeting the formation of outer-sphere P complexes, we should observe the same EM values for the systems containing 0.1 M NaCl regardless of P being present or not. This is not the case (Fig. 2). Therefore, our experimental evidence (shifts in IEP and EM with 25 and 50 μmol P and 0.1 M NaCl) suggests that P is specifically adsorbed (i.e., forms inner-sphere complexes) at the FH–water interface.

Another explanation for the observed EM shift of the P–FH samples is the formation of iron–phosphate (surface) precipitates, which might alter the charge properties of the FH. However, speciation calculations in MINEQL + (47) predict that all samples were undersaturated with respect to $FePO_4 \cdot 2H_2O$(s).

The EM measurement results are consistent with the results of the I effects on the P adsorption envelopes discussed in the previous section. It is, however, difficult to suggest molecular scale adsorption mechanisms based on our macroscopic data alone (the adsorption envelopes and the EM measurements). We therefore performed ATR–FTIR spectroscopic analyses to investigate the molecular scale P surface speciation at the FH–water interface.

ATR–FTIR Analysis

(A) Theoretical IR vibrations of phosphoric acid. A tetragonal penta-atomic molecule (e.g., PO_4^{3-}) exhibits four different vibrations (i) the symmetric stretching (A_1, v_1), (ii) the symmetric bending (E, v_2), (iii) the asymmetric stretching (F, v_3) and (iv) the asymmetric bending (F, v_4). The v_1 (nondegenerate symmetric stretching) and the v_3 (triply degenerate asymmetric stretching) vibration can be utilized to understand not only the molecular symmetry of the phosphoric acid (P) but also the coordination environments of the P adsorption complexes on metal oxide surfaces. Infrared spectra of P have been extensively investigated by several researchers (8, 9, 48, 49). Phosphate has several pK_a values ($pK_1 = 2.20$, $pK_2 = 7.2$, and $pK_3 = 12.3$) (50), and the protonation significantly affects the P molecular symmetry. In Table 1, we have summarized (i) the molecular symmetry and (ii) the number and the position of the v_1 and v_3 vibrations of the phosphoric acid at different pH values reported in previous studies. Figure 3 shows the IR spectra of P solution species which are reproduced based on Tejedor-Tejedor and Anderson's research (8).

Fully deprotonated phosphoric acid (PO_4^{3-}) at pH 11 has T_d symmetry. This tetrahedra molecule shows a single v_3 asymmetrical vibration (F_2) at $\cong$1006 cm^{-1}, and there is no activation of the v_1 vibration (Fig. 3). Monoprotonated (HPO_4^{2-}) species have C_{3v} symmetry and the v_3 vibration splits into two (E and A_1) at $\cong$1077 and 989 cm^{-1}. There is also v_1 band activation at $\cong$850 cm^{-1}. Further protonation results in the formation of

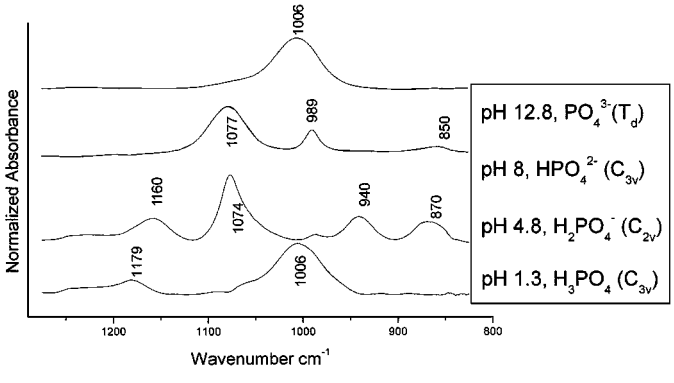

FIG. 3. ATR–FTIR spectra of phosphoric acid at different pHs.

TABLE 1
Position of IR Peak Maxima of Phosphoric Acid, P Adsorption Complexes on Iron Oxides, and Ferric Phosphate Solution Complexes

Species, symmetry, and reaction conditions[a]	Infrared active band positions (cm^{-1})			
	1100	1000	900	
PO_4^{3-} (aq), T_d (This study)		1006(v_3)		
HPO_4^{2-} (aq), C_{3v} (This study)		1077(v_3)	989(v_3)	850(v_1)
$H_2PO_4^-$ (aq), C_{2v} (This study)	1160(v_3)	1074(v_3)	940(v_3)	870(v_3)
H_3PO_4 (aq), C_{3v} (This study)	1179(v_3)	1006(v_3)		888(v_1)
Reference monodentate mononuclear complexes				
$Co(NH_3)_5PO_4$, C_{3v} (3)		1030(v_3)	980(v_3) 934(v_1)	
Reference bidentate binuclear complexes				
$(CH_3O)_2PO_2^-$, C_{2v} (3)	1220(v_3) 1110(v_3)	1050(v_3)		815(v_1)
$Co(NH_2CH_2CH_2NH_2)PO_4$, C_{2v} (3)		1085(v_3) 1050(v_3)	915(v_3) 900(v_1)	
Goethite-P (paste) (8)				
pH 4.5, 2.35 μmol m^{-2}	1121(v_3)	1044(shoulder) 1004(v_3 bands)	Peaks <940 cm^{-1} cannot be identified due to the absorption bands of goethite	
pH 4.5, 1.85 μmol m^{-2}	1095(v_3)	1044(v_3) 1004(v_3)		
pH 4.5, 1.23 μmol m^{-2}	1097(v_3)	1044 1004 (shoulder)(v_3 bands)		
pH 5–8.4, 1.85–2.35 μmol m^{-2}	≅1100(v_3)	≅1040(v_3) ≅1006(v_3)		
Goethite-P (in suspension) (6)				
pH 3.6–5.1, 1.25–2.5 μmol m^{-2}	≅1100(v_3) (Not well defined)	≅1000(v_3) (Not well defined)		
pH 8.1–9.7, 0.63–1.25 μmol m^{-2}		≅1080(v_3) ≅1040(v_3)		
Ferric phosphate monodentate mononuclear solution complexes				
FeH_2PO_4 or $FeHPO_4$ (8) pH 1, 14 mmol H_3PO_4, 0.8 mmol $Fe(ClO_4)_3$, 0.1 M $HClO_4$, 0.25 M $NaClO_4$	1170(v_3)	1077(v_3)	980(v_3)	
pH 1, 14 mmol H_3PO_4, 0.8 mmol $Fe(NO_3)_3$, 0.1 M HNO_3, 0.25 $MNaNO_3$ (8)	1149(v_3)	1085(v_3)	960(v_3)	
Ferric phosphate monodentate mononuclear (This study based on Rose *et al.*, (55))		1095(v_3) 1034(v_3)	986(v_3)	

[a] References are given in parenthesis.

diprotonated phosphate (i.e., $H_2PO_4^-$), which leads to a reduction in the symmetry from C_{3v} to the C_{2v}. The v_3 (E) vibration splits into two bands (B_1 and B_2), therefore, there are a total of three v_3 bands (B_1, B_2, and A_1) at ≅1160, 1074, and 940 cm^{-1}. The v_1 vibration shifts to higher wavenumber at ≅870 cm^{-1}. At pH ≅ 1.3, the symmetry of the dominant phosphoric acid species is $H_3PO_4(C_{3v})$ and the spectrum shows doublets (E and A_1) of the v_3 vibration at ≅1179 and 1006 cm^{-1}. In summary, the numbers of the v_3 vibration are two for the C_{3v} symmetry and three for the C_{2v} or lower (C_1) symmetry. The results of the P IR spectra are in good agreement with the studies by Chapman *et al.* (48) and Nakamoto (49).

The peak positions of several P model compounds and P adsorption complexes at iron oxide–water interfaces based on in situ FTIR studies are also summarized in Table 1. Although the band positions significantly differ between different P compounds, the numbers of bands with respect to the symmetry are consistent. This is also true for other P model compounds reported in Table 1. Atkinson and coworkers reviewed the v_1 and v_3 vibrations of the reference, monodentate mononuclear complex $Co(NH_3)_5PO_4$ (C_{3v}), and the reference bidentate binuclear complexes $(CH_3O)_2PO_2^-(C_{2v})$ and $Co(NH_2CH_2CH_2NH_2)PO_4(C_{2v})$ based on the studies by Kumamoto and Lincoln and Stranks (3, 51, 52). The number of the v_3 vibrations in these complexes is in good agreement with the predicted numbers based on the molecular symmetry (C_{3v} or C_{2v}) (Table 1).

We can apply the concept of molecular symmetry as related to changes in the v_3 and v_1 vibrations to P adsorption complexes on metal oxide surfaces. If orthophosphate ions (PO_4^{3-}) are coordinated with metal ion(s) at the hydroxide surface by forming inner-sphere complexes, one should observe a reduction in symmetry with respect to the free aqueous PO_4^{3-} (T_d). As the symmetry lowers from T_d to C_{3v} and to C_{2v}/C_1, the triply degenerate v_3 vibration splits into two or three bands, and the nondegenerate v_1 vibration shifts upon the changes in coordination environment (49). If P ions form outer-sphere complexes, the v_3 vibration of the free P ions at the same pH should be shifted slightly due to slight distortion in adsorbed P molecules via van der Waals forces, but there should be no influence on the number of v_3 vibrations.

To investigate the P surface complexes at the FH–water interface, we first compared the IR spectra of adsorbed species

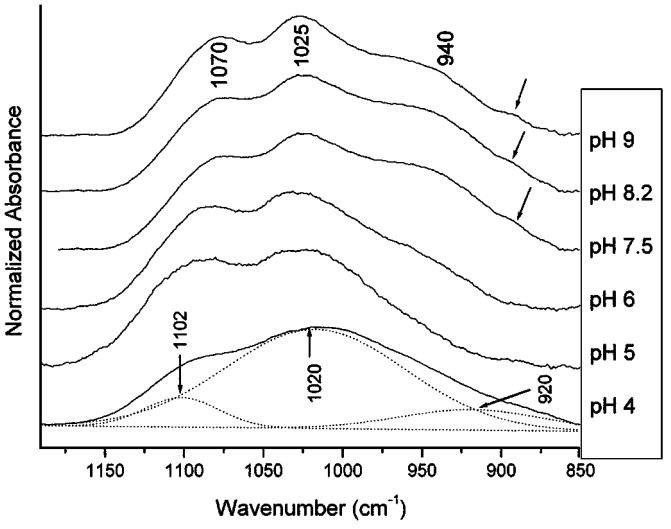

FIG. 4. ATR–FTIR spectra: pH effects (4–9) on the P adsorption complexes ($\Gamma = 0.38$ μmol m^{-2}) at the FH–water interface.

to the spectrum of the dominant phosphoric acid species at the same pH to distinguish the inner-sphere from the outer-sphere adsorption complexes. Second, we assigned the symmetry of the adsorption complexes based on the number of v_3 band splitting and/or the presence or absence of the v_1 vibration. Peak deconvolution and Gaussian profile fitting were performed to reveal the assemblage of multiple v_3 bands using the Peaksolve software package version 1.05 (Galactic Industries Corp.). This molecular symmetry assignment allows us to speculate on the molecular configurations of the surface complexes. Third, the spectra of the adsorption complexes in H_2O were compared with those in D_2O. If there are any shifts in the band position in these spectra, one can suggest that the surface complexes are associated with proton(s). Based on the combined information from these experiments, the final adsorption complexes can be proposed.

(B) pH effect on P adsorption complexes at pH 4–9. Figure 4 shows the pH effect on the P surface complexes for samples with the same loading level of $\Gamma = 0.38$ μmol m^{-2}. The highest peak at $\cong$1020 cm^{-1} for the sample reacted at pH 4 is slightly shifted to $\cong$1025 cm^{-1} with increasing pH from 4 to 9. The broad spectrum at pH 4 is an assemblage of three v_3 vibrations ($\cong$1102 and 1020 cm^{-1}, and at $\cong$920 cm^{-1}) (Fig. 4), as determined via Gaussian profile fit analysis. This indicates the C_{2v} or lower symmetry for the P adsorption complexes forming at this pH. The position of peak maxima ($\cong$1102 and $\cong$1020 cm^{-1}) is similar to the spectra of P on goethite surfaces in previous in situ FTIR studies (Table 1) (6, 8), suggesting similar P surface complexes might be forming at the FH/goethite–water interface.

As pH increases, the triplet splitting of the v_3 vibration becomes well resolved (Fig. 4). Interestingly, the spectra at pH 7.5, 8.2, and 9 show a small shoulder at $\cong$890 cm^{-1} (indicated by arrows in Fig. 4) that is probably the nondegenerate v_1 vibration of the C_{2v} or C_1 symmetry species. The presence of the v_1 vibration at pH > 7.5 will be discussed later. Overall, there are no significant changes in the IR spectra of the P surface complexes with changing pH, but the molecular symmetry seems to remain C_{2v} or lower (Fig. 4). It is clear that the inner-sphere adsorption of P causes the reduction in the molecular symmetry from T_d (PO_4^{3-}) to C_{2v} or lower. If the symmetry reduction is caused only by protonation, as would be the case for outer-sphere adsorption, then the v_3 vibrations should appear at similar wavenumbers for the dominant phosphoric acid species in the pH range studied (4–9) (i.e., $H_2PO_4^-$ and or HPO_4^{2-}). The peak maxima of the v_3 vibrations of the reacted samples, however, are significantly different from those of the P solution species (Figs. 3 and 4). Therefore, the symmetry reduction resulted from the P coordination onto iron octahedral structures at the FH surfaces, indicating the formation of P inner-sphere complexes. This is consistent with the results of the adsorption envelopes and the EM measurements. The type of adsorption complexes will be discussed in the next section.

(C) Loading level effects on P adsorption complexes at pH $\geq$ 7.5. The IR spectra of the P adsorption complexes ($\Gamma =$ 0.38, 1.15, 1.82, and 2.42 μmol m^{-2}) at pH 7.5 are shown in Fig. 5. All spectra show well-resolved triplet splitting of the v_3 vibration ($\cong$952, $\cong$1021, and $\cong$1088 cm^{-1}) as determined via Gaussian profile fit analysis, indicating C_{2v} or lower symmetry regardless of loading levels. The central peak at $\cong$1021 cm^{-1} is surrounded by two peaks ($\cong$1088 and 952 cm^{-1}) that are of near equal intensity (Fig. 5). The distribution and the peak intensity of the triplet splitting resemble those of the IR spectrum for $H_2PO_4^-$ (Fig. 3). Possible adsorption complexes can be postulated to be $\equiv$FeHPO$_4$ or $\equiv$Fe$_2$PO$_4$. The similar IR spectra can also be seen in the adsorption samples at pH 8.2 and 9 (Fig. 4). To further investigate the coordination and protonation environment of the P surface complexes,

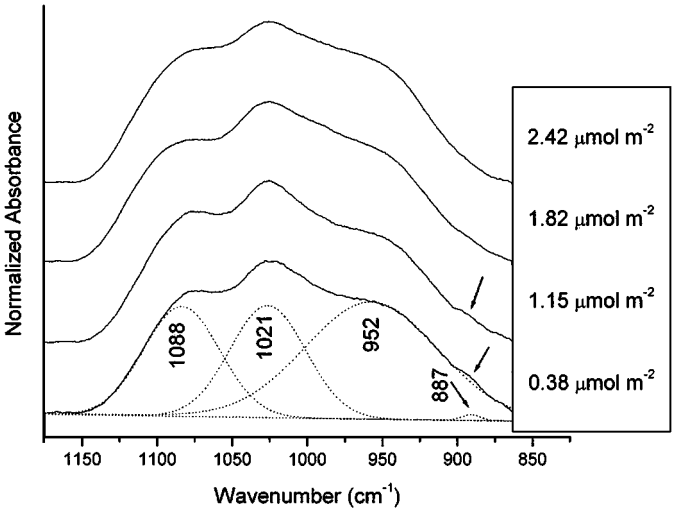

FIG. 5. ATR–FTIR spectra: loading level effect ($\Gamma = 0.38$–2.42 μmol m^{-2}) on the P adsorption complexes at pH 7.5 at the FH–water interface.

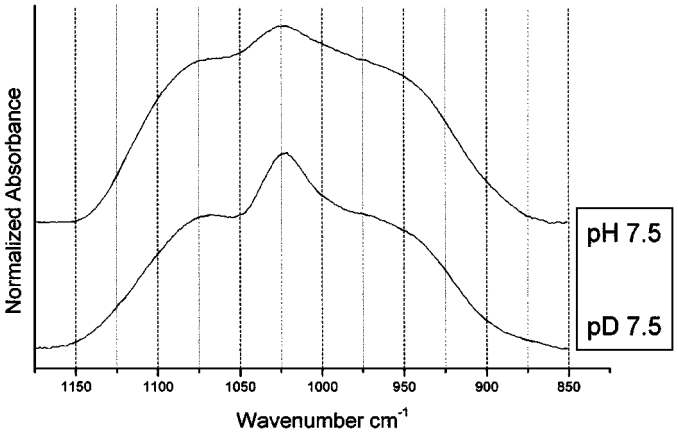

FIG. 6. ATR–FTIR spectra of P adsorption complexes at pH/pD 7.5 at the FH–water interface.

we compared the spectra at pH/pD 7.5 with the loading level of 2.42 μmol m^{-2} (Fig. 6). The spectra show no significant change in the position of the v_3 vibration at 850–1175 cm^{-1} (Fig. 6), indicating that the adsorption complexes are not associated with protons. Similar results were obtained in samples with loading levels of 0.38–1.82 μmol m^{-2} at pH $\geq$ 7.5 (not shown). The surface complexes that have the C_{2v} or lower symmetry without proton association are the nonprotonated bidentate binuclear complexes ($\equiv Fe_2PO_4$). We, therefore, suggest the predominant formation of the nonprotonated bidentate binuclear species at pH 7.5 at a loading level of 0.38–2.42 μmol m^{-2}. These data interpretations can be supported by comparing them to arsenate (AsO_4^{3-}) adsorption mechanisms at the FH–water interface at pH 8, since arsenate has similar chemical properties (e.g., pK_a) to phosphate. Waychunas and coworkers reported the formation of As(V), bidentate binuclear species based on extended X-ray absorption, fine structure spectroscopy (EXAFS) (53). A previous in situ FTIR study also showed similar triplet splitting of the v_3 vibration in the spectra for P adsorbed goethite surfaces (pH 6–8.3, Γ = 1.85–2.35 μmol m^{-2}) (Table 1), which was assigned to nonprotonated, bidentate binuclear complexes (8).

Interestingly, there is an activation of the v_1 vibration at $\cong$887 cm^{-1} in the low loading (Γ = 0.38 and 1.15 μmol m^{-2}) samples as determined via Gaussian profile fit analysis (Fig. 5). In Fig. 5, the small v_1 vibration becomes hidden when the loading level ranges from 0.38 to 2.42 μmol m^{-2} due to the shift and the intensification of the v_3 vibration at $\cong$950 cm^{-1}. The v_1 symmetrical vibration is observed in the loading level (Γ = 0.38–1.15 μmol m^{-2}) samples reacted at pH $\geq$ 7.5 (indicated by arrows in Figs. 4 and 5), but not in the samples reacted at pH < 7.5 (Figs. 4 and 7). The v_1 vibration can be possibly explained by (i) the presence of different surface complexes (e.g., monodentate mononuclear complexes) other than the predominant nonprotonated bidentate binuclear complexes and/or (ii) further distortion in the molecular symmetry of the predominant nonprotonated bidentate binuclear complexes. A mixture of surface complexes, therefore, might be forming at these pH and loading levels. In Fig 4, the peak at $\cong$1070 cm^{-1} becomes more intensified relative to the peak maxima at $\cong$940 cm^{-1} with increasing pH from 7.5 to 9. The slight changes in the peak intensity in v_3 vibrations ($\cong$940 and 1070 cm^{-1}) at pH $\geq$ 7.5 may suggest that the C_{2v} molecular symmetry is slightly lowered. If one can assume that the same surface species are present between pH 7.5 and 9, the distortion in the C_{2v} molecular symmetry could be caused by complexation with either protons or other ions from the bulk solution. Since the positions of the v_3 vibrations had no influence, after the deuterium exchange, between 850–1200 cm^{-1} in the samples at pH 7.5 (Fig. 6), the surface complexes are not associated with protons. Association with sodium ions may account for the molecular distortion observed at pH $\geq$ 7.5. As discussed in the adsorption envelope section, the Na^+ ions might be electrostatically attracted to the adsorbed P at the FH–water interface. This mechanism is indirectly supported by Nazyo's macroscopic evidence that Na^+ adsorption onto FH significantly increases from 0 to $\cong$1.12 μmol m^{-2} with increasing pH from 4.4 to 10.2 at a constant P loading level ($\Gamma \cong$ 0.29 μmol m^{-2}) on the FH surface (26).

We, therefore, suggest that the nonprotonated bidentate, binuclear complexes (Fe_2PO_4, C_{2v}) predominantly form at pH $\geq$ 7.5 at the FH–water interface under our experimental conditions. However, the presence of different surface complexes (e.g., monodentate mononuclear complexes) and/or $\equiv Fe_2PO_4 \cdots\cdots Na^+$ complexes cannot be excluded.

(D) Loading level effects on P adsorption complexes at pH < 7.5. Figure 7 shows the loading level effects on the P surface complexes at pH 4. The loading level does not seem to have a strong influence on the IR spectra, suggesting that the molecular symmetry of the P surface complexes is similar. To deconvolute the assemblage of peaks in these broad spectra, the Gaussian profile fit analyses were performed. The peak fitting analysis in the spectrum at pH 4 with Γ = 0.38 μmol m^{-2}

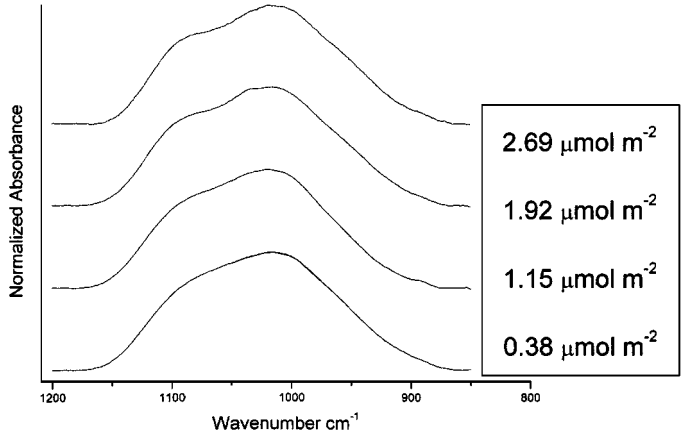

FIG. 7. ATR–FTIR spectra: loading level effect (Γ = 0.38–2.69 μmol m^{-2}) on the P adsorption complexes at pH 4 at the FH–water interface.

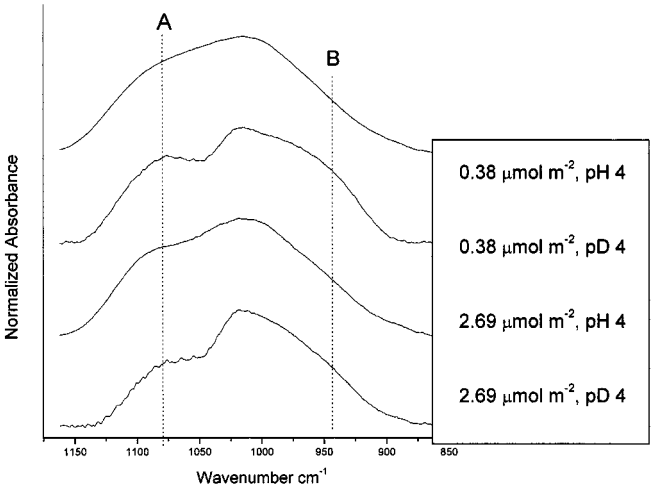

FIG. 8. ATR–FTIR spectra of P adsorption complexes at pH/pD 4 at the FH–water interface.

revealed that the broad peak was an assemblage of three υ_3 vibrations at ≅1102, 1020, and ≅920 cm^{-1} (bottom spectrum in Fig. 4), indicating the C_{2v} or lower symmetry. Similar results were obtained in samples at pH 4, 5, and 6 (not shown), indicating these surface complexes have C_{2v} or lower symmetry.

The P adsorption complexes at pD 4 with $\Gamma = 0.38$ and 2.69 μmol m^{-2} compared with those at pH 4 show that the peaks at pH 4 are shifted to ≅948 and 1077 cm^{-1} (dashed line A and B in Fig. 8) after deuterium exchange. These results suggest that the adsorption complexes forming at pH 4 and $\Gamma = 0.38-2.69$ μmol m^{-2} are associated with proton(s). As pH decreases below 7.5, protonation on the surface complexes can be expected. The protonation further lowers the symmetry of the P adsorption complexes to C_1. Based on the IR spectra assignment at pH ≥ 7.5 (i.e., nonprotonated, bidentate binuclear complexes), we can predict the type of adsorption complexes at pH < 7.5 to be protonated, bidentate binuclear complexes. In fact, Tejedore-Tejedore and Anderson (8) suggested that the nonprotonated bidentate binuclear complexes at pH > 6 become monoprotonated bidentate binuclear (≡Fe_2HPO_4) surface complexes with decreasing pH from 6.0 to 3.6 at the goethite-water interface.

It is possible, however, that the protonated, monodentate mononuclear complexes (≡$FePO_4H$ and ≡$FePO_4H_2$) and monodentate mononuclear complexes with hydrogen bonding with hydroxyl groups of the FH surface form, because they all have the C_{2v} or lower symmetry and are associated with proton(s) (Fig. 10). We, therefore, compare our IR spectra with the FTIR spectra of Fe–P monodentate aqueous complexes that were well-characterized by in situ spectroscopic techniques such as the spectrophotometric method and EXAFS. Wilhelmy *et al.* (54) studied the equilibra and kinetics of ferric and phosphate ion complexation at pH < 2 using spectrophotometric and stop-flow techniques. They suggested that $FeH_2PO_4^{2+}$ species are formed under the specific reaction conditions (0.014 M H_3PO_4, 0.1 mmol $Fe(ClO_4)_3$, 0.1 M $HClO_4$, 0.25 M $NaClO_4$ at pH 1). The IR spectrum of this complex was earlier reported by Tejedor-Tejedor and Anderson (8). The peak maxima of the triplet splitting of the υ_3 vibrations are reported in Table 1 and are consistent with C_{2v} or lower symmetry. The symmetry is in good agreement with the three υ_3 band splitting of either diprotonated monodentate mononuclear complexes ($FeH_2PO_4^{2+}$, C_1) or monoprotonated monodentate mononuclear complexes ($FeHPO_4^{2+}$, C_1).

The phosphorus K edge EXAFS spectroscopic study by Rose and coworkers (55) also showed the formation of monodentate mononuclear, ferric phosphate solution complexes. They investigated the local structural environment of phosphate during the hydrolysis of $FeCl_3$ in the presence of phosphate at pH < 1 with P/Fe = 0.5 and n = [OH]/[Fe] = 1 and found evidence for the formation of monodentate mononuclear Fe–PO_4 (aq) complexes (55). We determined the ATR–FTIR spectrum for the P species forming under the same reaction conditions as those of Rose *et al.* (55). The broad peak is an assemblage of three υ_3 vibrations positioned at 1100, 1028, and 971 cm^{-1} (Fig. 9), indicating C_{2v} or lower symmetry. Whereas EXAFS analysis are not sensitive to reveal the protonation environment of the PO_4 surface complexes, the molecular symmetry identification via FTIR analysis is sensitive to protonation of the P surface complexes. Several molecular symmetries are possible for this Fe–P monodentate mononuclear (aq) complex with C_{2v} or lower symmetry. They are monoprotonated monodentate mononuclear (C_1), diprotonated monodentate mononuclear (C_1), nonprotonated monodentate mononuclear with hydrogen bonded with the hydroxyl group of the FH (C_1), monoprotonated monodentate mononuclear with hydrogen bonded with the hydroxyl group of the FH (C_1), and diprotonated monodentate mononuclear with hydrogen bonded with the hydroxyl group of the FH (C_1) (Fig. 10c–10g).

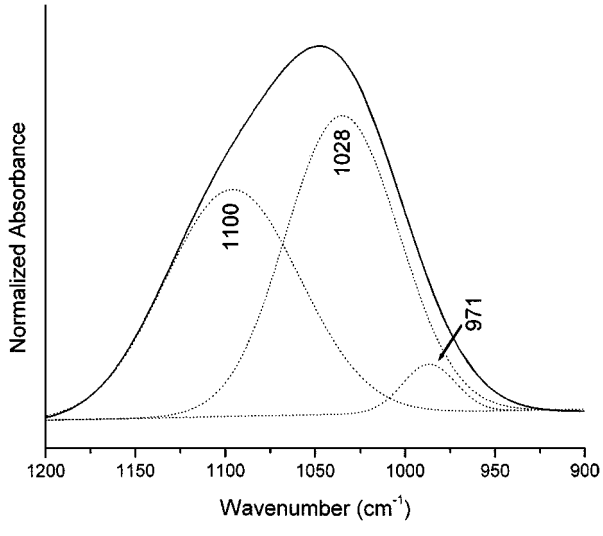

FIG. 9. Monodentate mononuclear Fe–P (aq) complex. The spectra show raw spectra and deconvolted peaks in solid line and the fitted profiles in dotted line.

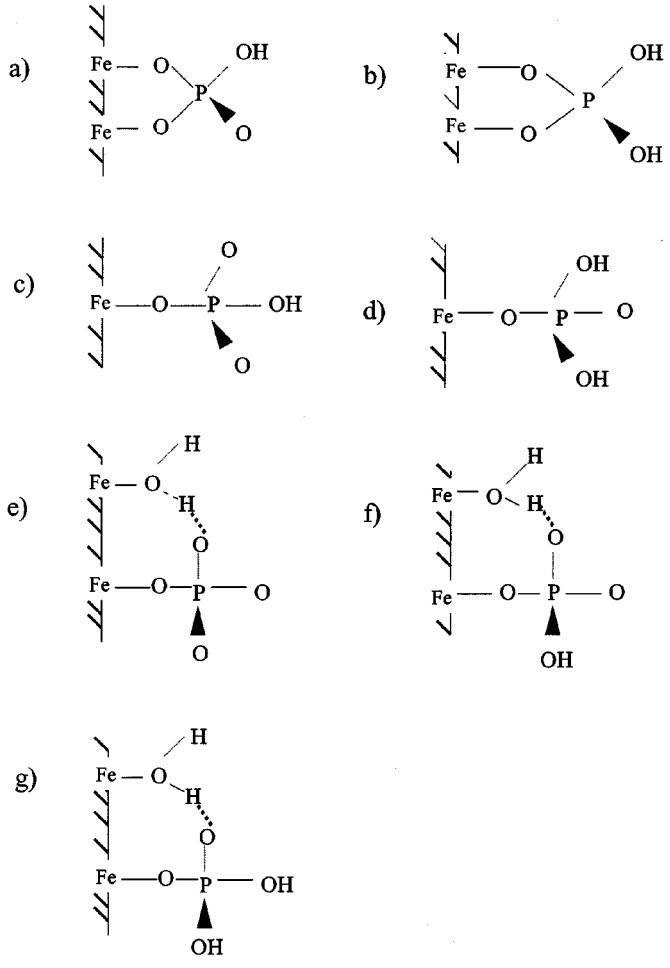

FIG. 10. Possible molecular configurations (C_{2v} or lower) of protonated P inner-sphere complexes at the FH–water interface. (a) monoprotonated bidentate mononuclear (C_1), (b) diprotonated bidentate mononuclear (C_{2v}), (c) monoprotonated monodentate mononuclear (C_1), (d) diprotonated monodentate mononuclear (C_1), (e) nonprotonated monodentate mononuclear with hydrogen bonded with the hydroxyl group of the FH (C_1), (f) monoprotonated monodentate mononuclear with hydrogen bonded with the hydroxyl group of the FH (C_1), and (g) diprotonated monodentate mononuclear with hydrogen bonded with the hydroxyl group of the FH (C_1).

Comparison of the peak positions of the monodentate mononuclear reference complexes to our experimental spectra at pH < 7.5 indicates no similarities. The peak at 920 cm^{-1} is only present in our IR spectra. This dissimilarity might suggest that the predominant complexes forming at pH 4 at the FH–water interface are unlikely to be mono-/diprotonated, monodentate mononuclear complexes. Assigning the type of surface complexes based on the band positions of the reference compounds, however, is risky because the position of bands could be shifted due to differences in the reaction conditions (e.g., loading levels, P/Fe ratio, and water content). Tejedore-Tejedor and Anderson (8) reported changes in the peak position with changing P loading levels (1.23–2.35 μmol m^{-2}) at the goethite–water interface at pH 4.5 (Table 1). The band position could be shifted with changing the moisture content. Several researchers have shown that the position and the intensity of the υ_3 vibration of oxyanions (phosphate and sulfate) can be altered by changing drying conditions (air dried, N_2 drying, and evacuation) (3, 6, 12). Elimination of the entrained water could facilitate transformation from low energy binding (outer-sphere and/or monodentate mononuclear complexes) to higher energy binding (bidentate binuclear) complexes. The IR spectra collected under dry and/or severely evacuated conditions must be carefully interpreted based on the purpose of the study. We, therefore, rely on the number of the υ_3 vibrations and the molecular symmetry of the P surface complexes more than on the positions of bands. In summary, it is possible that the protonated, monodentate mononuclear complexes, nonprotonated, monodentate mononuclear complexes with hydrogen bonding, and protonated, bidentate binuclear complexes are present at pH < 7.5 (Fig. 10).

CONCLUSION

The results of the P inner-sphere adsorption mechanisms are consistent based on adsorption envelopes, EM measurements and ATR–FTIR analysis. Based on our IR analysis, the predominant formation of the nonprotonated bidentate binuclear species (Fe_2PO_4) at pH > 7.5 is proposed and the surface complexes might co-exist with different surface species (e.g., monodentate mononuclear) and/or $\equiv Fe_2PO_4 \cdots\cdots Na$ at pH $\geq$ 7.5. The exact identity of the protonated P inner-sphere, surface complexes (i.e., protonated, monodentate mononuclear complexes and/or protonated, bidentate binuclear complexes) forming at pH < 7.5 could not be elucidated due to limitations in mid-IR range, FTIR analysis. In order to identify accurate P adsorption mechanisms in this pH range, local atomic structural information (P–Fe bond distances and the coordination number) of the adsorbed P via phosphorus EXAFS analysis would be very useful to distinguish the protonated, monodentate mononuclear from the protonated, bidentate binuclear complexes. These analyses would also be useful in determining the formation of iron phosphate surface precipitates that could not be well evaluated by ATR–FTIR analysis. In previous in situ FTIR studies on P adsorption at the goethite–water interface (6, 8), peak fitting analysis on P υ^3 vibrations and deuterium exchange experiments on P surface complexes were neglected. Therefore, the P molecular symmetry of adsorption complexes with respect to protonation and surface complexation was not clearly understood. Our comprehensive in situ ATR–FTIR study, however, revealed not only P bonding mechanisms at the FH–water interface but also the protonation of surface complexes. Such detailed molecular scale information should greatly enhance surface complexation modeling of P adsorption reactions at the mineral–water interface. While our findings (e.g., inner-sphere bidentate binuclear complexes) provide important information on P surface speciation at the FH–water interface for reaction times of less than 48 h; longer residence time effects (months to years) on P adsorption mechanisms at the FH–water interface are not well understood. It is possible that longer contact times could result in nonsingular

reactions due to chemical reconfiguration reactions, if biotic and abiotic reductive dissolution of adsorbate are inhibited. Aging effects on P surface speciation at the FH–water interface could be further investigated using time-resolved in situ spectroscopic techniques; such studies could provide insights on reactions in natural systems (e.g., long-term P amended soils and sediments).

ACKNOWLEDGMENTS

The authors are grateful to the USGS for financial support of this research and E. J. Elzinga and R. G. Ford for their critical review of the manuscript. Y. A. appreciates the receipt of a College of Agricultural and Natural Resources Graduate Research Assistantship and expresses gratitude to Dr. S. Dentel and C. A. Walker for assistance with the EM measurements and to Dr. R. Maynard of DuPont Co. for assistance with the surface area analysis of FH.

REFERENCES

1. Ryden, J. C., Syers, J. K., and Harris, R. F., *in* "Advances in Agronomy," Vol. 25, p. 1, 1973.
2. Vaithiyanathan, P., and Correll, D. L., *J. Environ. Qual.* **21,** 280 (1992).
3. Atkinson, R. J., Parfitt, R. L., and Smart, R. S. C., *J. Chem. Soc. Faraday Trans. 1* **70,** 1472 (1974).
4. Nanzyo, M., and Watanabe, Y., *Soil Sci. Plant Nutr.* **28,** No. 3, 359 (1982).
5. Parfitt, R. L., Russell, J. D., and Farmer, V. C., *J. Chem. Soc. Faraday Trans.* **172,** 1082 (1976).
6. Parfitt, R. L., and Atkinson, R. J., *Nature.* **264,** No. 30, 740 (1976).
7. Parfitt, R. L., Atkinson, R. J., and Smart, R. S. C., *Soil Sci. Soc. Am. Proc.* **39,** 837 (1975).
8. Tejedor-Tejedor, M. I., and Anderson, M. A., *Langmuir* **6,** 602 (1990).
9. Persson, P., Nielsson, N., and Sjöberg, S., *J. Colloid Interface Sci.* **177,** 263 (1996).
10. Goldberg, S., and Sposito, G., *Commun. Soil Sci. Plant Anal.* **16,** No. 8, 801 (1985).
11. Goldberg, S., and Johnston, C. T., *J. Colloid Interface Sci.* **234,** 204 (2001).
12. Hug, S. J., *J. Colloid Interface Sci.* **188,** 415 (1997).
13. Peak, D., Ford, R. G., and Sparks, D. L., *J. Colloid Interface Sci.* **218,** 289 (1999).
14. Schulthess, C. P., Swanson, K., and Wijnja, H., *Soil Sci. Soc. Am. J.* **62,** No. 1, 136 (1998).
15. Wijnja, H., and Schulthess, C. P., *J. Colloid Interface Sci.* **229,** 286 (2000).
16. Fuller, C. C., and Davis, J. A., *Nature* **340,** 52 (1989).
17. Jackson, T. A., and Keller, W. D., *Am. J. Sci.* **269,** 446 (1970).
18. Schwertmann, U., Schulze, D. G., and Murad, E., *Soil Sci. Soc. Am. J.* **46,** 869 (1982).
19. Schwertmann, U., and Taylor, R. M., *in* "Minerals in Soil Environments" (J. B. Dixon and S. B. Weed, Eds.), p. 379. Soil Science Society of America, 1989.
20. Parfitt, R. L., *J. Soil Sci.* **40,** 359 (1989).
21. Willett, I. R., Chartres, C. J., and Nguyen, T. T., *J. Soil Sci.* **39,** 275 (1988).
22. Barron, V., Galvez, N., Jr., M. F. H., and Torrent, J., *Am. Mineral.* **82,** 1091 (1997).
23. Kandori, K., Uchida, S., Kataoka, S., and Ishikawa, T., *J. Mater. Sci.* **27,** 719 (1992).
24. Biber, M. V., Afonso, M. D. S., and Stumm, W., *Geoch. Cosmochim. Acta.* **58,** No. 9, 1999 (1994).
25. Bondietti, G., Sinniger, J., and Stumm, W., *Colloids Surf.* **79,** 157 (1993).
26. Nanzyo, M., *Soil Sci. Plant Nutr.* **32,** No. 1, 51 (1986).
27. Schwertmann, U., and Cornell, R. M., "Iron Oxides in the Laboratory: Preparation and Characterization." VCH, Weinheim/New York, 1991.
28. Zelazny, L. W., He, L., and Vanwormhoudt, A., *in* "Methods of Soil Analysis Part 3-Chemical Methods" (D. L. Sparks, Ed.), p. 1231. Soil Science Society of America, 1996.
29. He, Z. L., Baligar, V. C., Martens, D. C., and Ritchely, K. D., *Soil Sci. Soc. Am. Proc.* **62,** 1538 (1998).
30. Murphy, J., and Riley, J. P., *Anal. Chim. Acta* **27,** 31 (1962).
31. Hiemenz, P. C., and Rajagopalan, R., "Electrophoresis and Other Electrokinetics Phenomena." Dekker, New York, 1997.
32. Rose, J., Manceau, A., Bottero, J., Manion, A., and Garcia, F., *Langmuir* **12,** 6701 (1996).
33. Barrow, N. J., Bowden, J. W., Posner, A. M., and Quirk, J. P., *Aust. J. Soil Res.* **18,** 395 (1980).
34. Edzwald, J. K., Toensing, D. C., and Leung, M. C., *Environ. Sci. Technol.* **10,** No. 5, 485 (1976).
35. Helyar, K. R., Munns, D. N., and Burau, R. G., *J. Soil Sci.* **27,** 307 (1976).
36. Helyar, K. R., Munns, D. N., and Burau, R. G., *J. Soil Sci.* **27,** 315 (1976).
37. Kafkafi, U., Bar-Yosef, B., Rosenberg, R., and Sposito, G., *Soil Sci. Soc. Am. J.* **52,** 1585 (1988).
38. Ryden, J. C., Syers, J. K., and Mclaughlin, J. R., *J. Soil Sci.* **28,** 62 (1977).
39. Ryden, K. C., and Syers, J. K., *J. Soil Sci.* **26,** 395 (1975).
40. Hayes, K. F., Papelis, C., and Leckie, J. O., *J. Colloid Interface Sci.* **125,** No. 2, 717 (1988).
41. Bowden, J. W., Nagarajah, S., Barrow, N. J., Posner, A. M., and Quirk, J. P., *Aust. J. Soil Res.* **18,** 49 (1980).
42. McBride, M. B., *Clays Clay Miner.* **45,** No. 4, 598 (1997).
43. Goldberg, S., and Sposito, G., *Soil Sci. Soc. Am. J.* **48,** 779 (1984).
44. Hansmann, D. D., and Anderson, M. A., *Environ. Sci. Technol.* **19,** 544 (1985).
45. Hunter, R. J., *in* "Colloid Science, A Series of Monographs," Vol. 219. Academic Press, San Diego, 1981.
46. Suarez, D. L., Goldberg, S., and Su, C., *in* "Mineral-Water Interfacial Reactions Kinetics and Mechanisms" (D. L. Sparks and T. J. Grundl, Eds.), ACS Symp. Series 715, Vol. 136. Am. Chem. Soc., Washington, DC, 1998.
47. Schecher, W. D., and McAvoy, D. C., "MINEQL + Environmental Research Software," 1998.
48. Chapman, A. C., and Thirlwell, L. E., *Spectrochim. Acta.* **20,** 937 (1964).
49. Nakamoto, K., "Infrared and Raman Spectra of Inorganic and Coordination Compounds." Wiley, New York, 1997.
50. Snoeyink, V. L., and Jenkins, D., Precipitation and dissolution. *in* "Water Chemistry," p. 243. Wiley, New York, 1980.
51. Kumamoto, J., *Spectrochim. Acta* **21,** 345 (1965).
52. Lincoln, S. F., and Stranks, D. R., *Aust. J. Chem.* **21,** 37 (1968).
53. Waychunas, G. A., Rea. B. A., Fuller, C. C., and Davis, J. A., *Geoch. Cosmochim. Acta* **57,** 2251 (1993).
54. Wilhelmy, R. B., Patel, R. C., and Matijevic, E., *Inorg. Chem.* **24,** 3290. (1985).
55. Rose, J., Flank, A., Masion, A., Bottero, J., and Elmerich, P., *Langmuir* **13,** 1827 (1997).